Magnetic frustration driven high thermoelectric performance in the kagome antiferromagnet YMn_6Sn_6

Honghui Wang,[1] Linfeng Jiang,[1] Zizhen Zhou,[1] Rui Wang,[1] Aifeng Wang,[1] Yisheng Chai,[1] Mingquan He,[1] Guang Han,[2] Jianjun Ying,[3] Xu Lu,[1] Yu Pan,[4] Guoyu Wang,[2] Xiaoyuan Zhou,[1,*] and Xianhui Chen[3,5,6]

[1]*College of Physics and Center of Quantum Materials & Devices, Chongqing University, Chongqing 401331, People's Republic of China*

[2]*College of Materials Science and Engineering, Chongqing University, Chongqing 400044, People's Republic of China*

[3]*CAS Key Laboratory of Strongly-coupled Quantum Matter Physics, and Department of Physics, University of Science and Technology of China, Hefei, Anhui 230026, People's Republic of China*

[4]*Max Planck Institute for Chemical Physics of Solids, 01187 Dresden, Germany*

[5]*High Magnetic Field Laboratory of the Chinese Academy of Sciences, Hefei, Anhui 230031, People's Republic of China*

[6]*Collaborative Innovation Center of Advanced Microstructures, Nanjing University, Nanjing 210093, People's Republic of China*

(Received 4 June 2023; revised 15 September 2023; accepted 9 October 2023; published 20 October 2023)

The introduction of magnetism has profound impacts on the thermodynamics of the carriers and thus thermoelectric (TE) performance, broadening the scope of traditional TEs. Herein, it is demonstrated that the large magnetic entropy induced by the interplanar magnetic frustration of an antiferromagnetic kagome lattice significantly enhances the Seebeck coefficient S in a broad temperature range, from around 50 K to above 380 K, which far exceeds those of other materials reported so far. Specifically, at 300 K and 9 T, the S and power factor (PF) is increased by 9.5 μVK^{-1} and 57%, respectively. In addition, a phonon drag contribution to the S is also observed around the phonon peak, which is confirmed by the fitting of thermal conductivity and heat capacity. Combining the contribution of both magnetic frustration and phonon drag, the maximum PF reaches 10.5 $\mu W\,cm^{-1}\,K^{-2}$ and is comparable to those of state-of-the-art conventional TE materials. This work supports the enhancement of TE performance through the magnetic frustration of an antiferromagnetic kagome lattice and phonon drag, and also discovers a potential new TE material system.

DOI: 10.1103/PhysRevB.108.155135

I. INTRODUCTION

Thermoelectric (TE) technology has attracted intensive attention because of the ability to realize direct conversion between electricity and heat. Since the Seebeck effect was discovered in 1822, a number of strategies have been implemented to enhance TE performance, mainly including band and phonon engineering [1–5], which drive the rapid development of TE materials. However, progress seems to have reached a plateau, and limited performance still prevents a large-scale application of TE technology. Thus, an urgent task is to enhance TE performance further by developing some novel and efficient routes. Although a traditional perspective has been devoted to eliminate magnetism to maintain high carrier mobility and attain excellent electrical transport performance, some recent results have confirmed that magnetism can play a more important role in enhancing the Seebeck coefficient S and thus TE performance [6–13]. For this reason, the introduction of magnetism becomes one of the most potential strategies to improve TE performance further.

A prerequisite for excellent TE materials is that they have a strong Seebeck effect, which describes the generation of an induced TE voltage in response to a temperature difference across the materials. For magnetic systems, the S originating from the spin-dependent contribution can be approximately understood through the purely thermodynamic Kelvin formula $S = (-1/e)d\mu/dT$, where e is the free charge [14]. Furthermore, the chemical potential μ is related to the derivative of the total electronic entropy Σ with carriers' number N of the system, i.e., $d\mu/dT = d\Sigma/dN$ [14,15]. Compared with nonmagnetic materials, the introduction of magnetism can enhance the electronic heat capacity (C_p) and, thus, total electronic entropy, which ultimately enhances the S and thus potentially improves TE performance [10,14,15]. For example, paramagnon drag drastically increases the S of lithium-doped MnTe and results in the TE figure of merit $ZT > 1$ through combining band engineering at 900 K [9]; spin fluctuation pronouncedly enhances the S of the weak, itinerant ferromagnet $Fe_{2.2}V_{0.8}Al_{0.6}Si_{0.4}$ and thus boosts the power factor (PF) by 20% around room temperature [10]; the superparamagnetic state induced by embedding nanoparticles of a soft magnetic material enables the dual control of electrical and thermal transport properties in optimizing TE performance of $Co_x/Ba_{0.3}In_{0.3}Co_4Sb_{12}$ [11]; and spin entropy induced by geometric magnetic frustration contributes a ten-times Sommerfeld value to the S in Na_xCoO_2 [12,13]. Therefore, introducing magnetism can play an important role in improving TE performance, and possibly further enhances TE performance beyond band and phonon engineering.

Lattice geometry and crystal symmetry are the key factors in determining physical properties of crystals. The kagome

*xiaoyuan2013@cqu.edu.cn

lattice is one typical example, composed of a two-dimensional network with corner-sharing triangles. It has attracted significant attention as it offers a great opportunity to explore intertwining geometry, topological bands, and electron order [16–24]. Owing to its unique lattice geometry, the kagome lattice has exhibited numerous novel physical phenomena, including magnetic frustration, superconductivity, charge-density waves, the anomalous Hall effect, the anomalous Nernst effect, and so on [16–25]. An antiferromagnetically coupled spin system on the kagome lattice is highly frustrated and exhibits a quantum disordered spin liquid state or a novel magnetically ordered state with nontrivial spin textures [16,26,27]. Thus, such a system provides fertile ground for investigating novel phenomena. However, the correlation between the unique magnetic properties of an antiferromagnetically coupled kagome lattice and its TE properties remains unclear.

RMn_6Sn_6 (R = rare earth element) is a typical kagome magnet. Its in-plane exchange interaction is strongly ferromagnetic [26]. However, the magnetic dynamics is controlled by an interplanar exchange interaction due to the Mermin-Wagner theorem, i.e., the ferromagnetic order in two-dimensional planes is strongly suppressed [26]. In this family, YMn_6Sn_6 exhibits an antiferromagnetic (AFM) interaction and a high magnetic frustration between layers [26]. Herein, we report the TE properties of YMn_6Sn_6, an antiferromagnetically coupled kagome lattice. The strong magnetic frustration and phonon drag greatly enhance its S and PF over a broad temperature range. The enhanced PF is comparable to that of state-of-the-art TE materials. Our work verified that YMn_6Sn_6 is a decent TE material, and may inspire the discovery of more novel high-performance TE materials in a frustrated AFM kagome lattice.

II. EXPERIMENT

The YMn_6Sn_6 single crystal was synthesized through a self-flux method [26,27]. After the growth of a single crystal, the quality and orientation were characterized by x-ray diffraction (XRD). Resistivity, the Seebeck coefficient, thermal conductivity, and heat capacity were measured using a PPMS-9T system (Quantum Design).

III. RESULTS AND DISCUSSION

YMn_6Sn_6 crystallizes in a hexagonal crystal structure with the space group $P6/mmm$ and consists of a Mn_3Sn kagome plane with alternating Sn_3 and Sn_2Y layers, as shown in Figs. 1(a) and 1(b). All manganese planes and in-plane nearest-neighbor Mn-Mn bonds are crystallographically equivalent. In comparison, the interplanar Mn-Mn bonds along c-axis are significantly different, exhibiting a ferromagnetic exchange interaction along Mn_3Sn-Sn_3-Mn_3Sn and an AFM exchange interaction along Mn_3Sn-Sn_2Y-Mn_3Sn, which result in high magnetic frustration through a second-neighbor interaction and thus a complex magnetic phase [26]. On cooling, as shown in Fig. 1(c), the manganese moments initially form a commensurate AFM phase around 340 K, and then an incommensurate AFM (IAFM) spiral phase appears below 333 K, which coexists with the commensurate

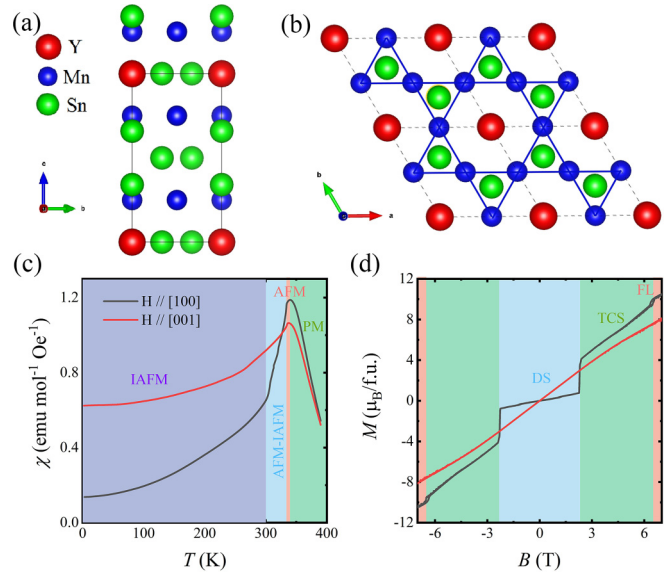

FIG. 1. (a) and (b) Schematic illustration of the crystal structure of YMn_6Sn_6. (c) The temperature dependence of susceptibilities with a magnetic field of 5000 Oe applied along [100] and [001], respectively. (d) Isothermal magnetizations M with a magnetic field applied along [100] and [001] at 2 K, respectively.

AFM phase above 300 K and becomes the only magnetic phase below 300 K [26]. In addition, multiple magnetic transitions appear in the process of the magnetic field driving the magnetic ground state into a ferromagnetic state, including a distorted spiral (DS) state, a transverse conical spiral (TCS) state, and a fan-like (FL) state, as shown in Fig. 1(d) [26].

The magnetic frustration yielded by the interplanar competing magnetic interactions induces not only a complex magnetic phase, but also possibly large magnetic entropy. Thus, according to the Kelvin formula [14], the strong magnetic frustration may significantly improve the S through the enhanced total entropy, and thus TE performance, as observed in chromium-doped $Fe_2VAl_{0.9}Si_{0.1}$ with a 20% improvement in the PF [10]. Based on this reason, the S of YMn_6Sn_6 was measured in the temperature range from 2 K to 380 K and under the magnetic field ranging from 0 T to 9 T. Figure 2(a) exhibits the temperature dependence of $S(T)_{\perp}$ with the magnetic field applied along the [001] crystal direction and the heat current along the [100] crystal direction. The zero-field $S(T)_{\perp}$ initially increases with decreasing temperature and reaches its maximum of 41 μVK^{-1} at 300 K, which is a very high value for a metallic system with a carrier density of $\sim 10^{22}$ cm^{-3} [28], and then starts to decrease and exhibits a kink around 49 K. After applying the magnetic field, the $S(T)_{\perp}$ gradually decreases with an increasing magnetic field in the high-temperature range and is almost independent of the magnetic field in the lower temperature range. In addition, the temperature range in which $S(T)_{\perp}$ is independent of the magnetic field gradually decreases with an increasing magnetic field. In order to exclude the contribution of the Lorenz force, the $S(T)_{//}$ was also performed with both the magnetic field and the heat current applied along the [100] crystal direction, which exhibits a similar magnetic field dependence behavior with $S(T)_{\perp}$. However, the change in $S(T)_{//}$ is slightly more

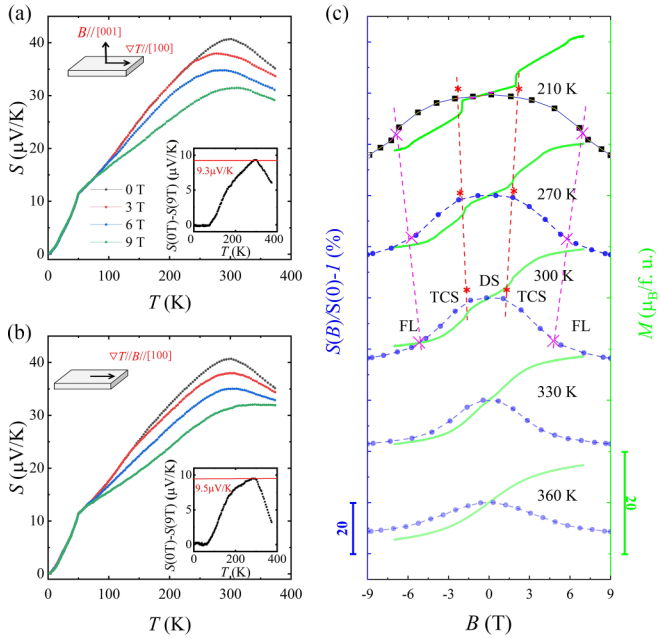

FIG. 2. (a) and (b) The magnetic field dependence of $S(T)$ with a heat current applied along the [100] crystal direction and a magnetic field applied along the [001] and [100] crystal directions in the temperature range from 2 K to 380 K, respectively. (c) The magnetic field dependence of $S(B)/S(0)$–1 (dotted/dashed lines) and M (solid green lines) with a magnetic field and heat current applied along the [100] crystal direction in the temperature range from 210 K to 360 K.

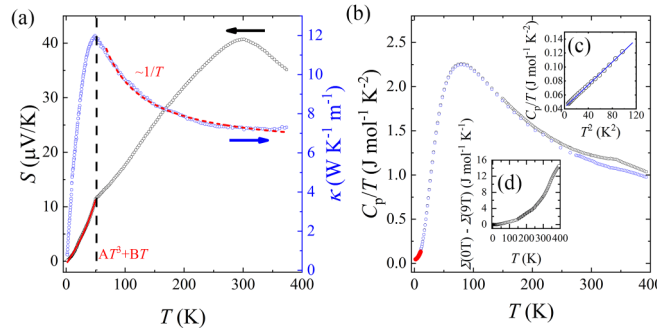

FIG. 3. (a) The temperature dependence of the S (black) and thermal conductivity (blue). The red solid and dashed lines indicate the fitted S through formulas $AT^3 + BT$ and $1/T$, respectively. (b) The temperature dependence of C_p/T in the temperature range from 2 K to 380 K. The red dots indicate the perfectly fitted C_p through the formula AT^3, as shown in inset (c), and C_p/T versus T^2 show a linear dependence in the temperature range from 2 K to 10 K. Inset (d) shows the temperature dependence of the magnetic entropy in the temperature range from 2 K to 380 K.

rapid with an increasing magnetic field, as shown in the insets of Figs. 2(a) and 2(b). The maximum of $S(0\,\mathrm{T})_{//}$–$S(9\,\mathrm{T})_{//}$ reaches 9.5μV K^{-1} at 300 K. The trend of the magnetic field dependence of $S(T)_{//}$ and $S(T)_{\perp}$ are consistent with the diagram of the S enhanced by magnetic frustration. The gradual decrease of $S(T)_{//}$ and $S(T)_{\perp}$ is due to the fact that the increasing magnetic field gradually suppresses magnetic entropy induced by magnetic frustration, which is clearer through $S_{//}(B)$, as shown in Fig. 2(c). Increasing the magnetic field gradually suppresses the magnetic frustration, leading to two clear transitions below 300 K on the M-H curves, corresponding to the DS-to-TCS states and the TCS-to-FL states, respectively. At the same time, the increasing magnetic field also makes the $S_{//}(B)$ gradually decrease and undergo two transitions, which are consistent with previous work [25]. Furthermore, the magnetic field thresholds for new magnetic phases gradually increase with decreasing temperature, in line with the change of the temperature dependence of $S_{//}(B)$. These results further suggest that the large magneto-Seebeck effect is closely related to the interplanar magnetic frustration in the antiferromagnetic kagome lattice YMn_6Sn_6.

There are still several questions that need to be clarified for the $S(T)$ and $S(B)$. First, the maximum of $S(T)$ appears at 300 K, but not at the antiferromagnetic ordered temperature. Through the magnetic field dependence of $S(T)$, under a magnetic field of 9 T, the S has the largest change at 300 K, suggesting that the magnetic frustration is possibly strongest at this temperature. In addition, a previous report [26] confirmed that the incommensurate magnetic state had more nearly equal wave vectors at 300 K, which may offer larger magnetic entropy. Thus, the occurrence of a maximum $S(T)$ at 300 K is more likely due to the presence of larger magnetic entropy induced by stronger magnetic frustration at 300 K than at other temperatures.

Second, the temperature dependence of the S around 49 K exhibits an obvious kink. Some reasons may be considered, including a magnetic/structural phase transition, the presence of strong electronic correlations, or an interaction of the phonon with the mobile charge carriers. Since there is no anomaly in the temperature dependence of heat capacity and M near 49 K, we claim that the kink in the S can hardly be due to a magnetic/structural phase transition. In order to explore the origins, we also measured the temperature dependence of thermal conductivity (κ) [Fig. 3(a)]. $\kappa(T)$ initially increases and then decreases (with an $\sim 1/T$ behavior due to phonon-phonon scattering), showing a peak value around 49 K, which is the same as the characteristic temperature of the kink in $S(T)$, further suggesting that the kink of $S(T)$ is related to phonon-related mechanisms. One of the origins related to the phonon that should be considered is the magnetoelastic coupling effect, which is widely found in rare earth compounds [29,30]. However, the temperature dependence of the change in cell parameters is not obviously abnormal, indicating that the magnetoelastic coupling effect is absent or extremely weak in YMn_6Sn_6 [31]. Furthermore, as shown by the solid red line in Fig. 3(a), $S(T)$ can be fitted through the formula $aT^3 + bT$ in the temperature range from 2 K to 49 K, suggesting that $S(T)$ is simultaneously contributed by both the diffusion part and the magnon/phonon drag part. As $S(T)$ is independent with magnetic field around the kink, the phonon drag part should be dominant. Phonon drag can be understood as an effect arising from a preferential scattering of the charge carriers by phonons in the direction of the heat flow. Usually, the phonon drag effect is strong near the temperature corresponding to the peak in thermal conductivity [32]. Figure 3(b) also shows the temperature dependence of C_p/T in the temperature range from 2 K to 250 K. C_p/T versus T^2 shows a linear

behavior in the temperature range of 2 K to 10 K [Fig. 3(b), inset 3(c)]. Thus, we can fit the low-temperature heat capacity by the formula $C_p/T = \gamma + \beta T^2$, where γ is the Sommerfeld coefficient. The values of γ and β are 0.04286 mJ mol^{-1} K^{-2} and 0.08071 mJ mol^{-1} K^{-2}, respectively. Based on this discussion, the Debye temperature of 416 K is calculated through the formula $\Theta_D = (12\pi^4 Rn/5\beta)^{1/3}$, where R is the molar gas constant and n is the number of atoms in a formula unit. Thus, the temperature corresponding to the peak of the thermal conductivity is $\frac{1}{8}$ of the Debye temperature. Combining the $1/T$ behavior of $\kappa(T)$ after the peak temperature, the peak in the thermal conductivity should be the phonon peak [33].

Third, besides the spin-dependent contribution, the change in the magnetic structure driven by the magnetic field also possibly changes the band structure and thus the magnetic-field dependence of $S(T)$. For example, in the magnetic semiconductor $Mn_3Si_2Te_6$, the external magnetic field induces a topological transition from a semiconductor to a nodal-line semimetal, which leads to a reduction in the S [34]. However, the change in $S(B)$ of YMn_6Sn_6 is more rapid at 300 K than 330 K, and YMn_6Sn_6 exhibits a more rapid transition into the ferromagnetic state at 330 K [26,27]. Thus, the reduction in $S(B)$ with an increasing magnetic field is not consistent with the scenario of the changed band structure driven by a magnetic field. To confirm further the origin of the magnetic field dependence of $S(T)$, as shown in Fig. 3(b), inset (d), the change of magnetic entropy $[\Sigma(0\,\mathrm{T})–\Sigma(9\,\mathrm{T})]$ is also calculated through $\Sigma = \int C_p/T\,dT$ based on the temperature dependence of the heat capacity under a magnetic field of 0 T and 9 T [Fig. 3(b)]. The significant magnetic entropy can be observed around 50 K, which is consistent with the magnetic frustration enhanced S scenario.

Surprisingly, because of competing magnetic interactions, the S is greatly enhanced by the magnetic frustration of the antiferromagnetic kagome lattice in an extremely broad temperature range from around 50 K to above 380 K, which is different from the traditional magnetic fluctuation that only exists in a narrow temperature zone around the magnetic transition temperature and is quickly quenched below the magnetic transition temperature. Therefore, the magnetic frustration exhibited in this work is more suitable for the practical application of relevant TE devices. Furthermore, in order to calculate the PF of antiferromagnetic YMn_6Sn_6, the temperature dependence of resistivity $\rho(T)$ was also measured under a different magnetic field, as shown in Figs. 4(a) and 4(b). $\rho(T)$ shows a metallic behavior over the entire temperature range, and slightly decreases under the magnetic field. Surprisingly, the magneto-ρ $[\rho_{//}(0\,\mathrm{T})/\rho_{//}(9\,\mathrm{T})–1 = 9.1\%$ at 300 K] is much smaller than magneto-S $[\ S_{//}(0\,\mathrm{T})/S_{//}(9\,\mathrm{T})–1 = 24.4\%$ at 300 K], as shown in Figs. 2(c) and Supplemental Material Fig. S3 [35], which is more advantageous for obtaining a high PF. As stated by Roychowdhury *et al.* [25], the effect of spin scattering is usually weak in magneto-S. However, the magneto-S is significantly larger than magneto-ρ in YMn_6Sn_6, which further suggests that the large S does not originate from spin scattering. The diagram of magnetic entropy induced by magnetic frustration enhancing S is probably more reasonable in YMn_6Sn_6. Based on the measurement of $S(T)$ and $\rho(T)$ shown in Figs. 2(a) and 4(b) and 4(a) and 4(b),

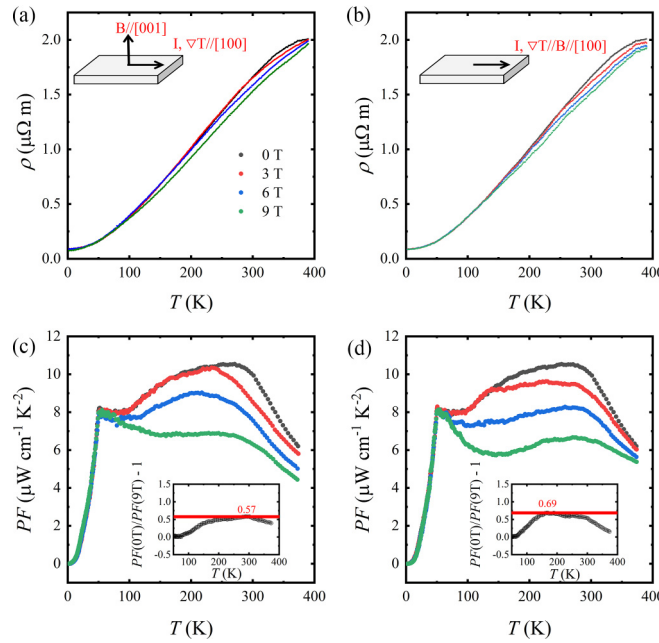

FIG. 4. (a) and (b) The temperature dependence of resistivity with an electric current applied along the [100] crystal direction and a magnetic field applied along the [001] and [100] crystal directions, respectively. (c) and (d) The temperature dependence of the power factor with heat/electric current applied along the [100] crystal direction and a magnetic field applied along the [001] and [100] crystal directions, respectively. Insets: The magneto-PF [PF(0)/PF(B)–1] under a magnetic field of 9 T.

we calculated the PF (S^2/ρ), which characterizes the power output capacity of the TE materials, as shown in Figs. 4(c) and 4(d). The zero-field PF shows a weak temperature dependence between 49 K and 380 K, and quickly decreases below 49 K. The maximum PF reaches 10.5 μ W cm^{-1} K^{-2} around 270 K, which is comparable with those of state-of-the-art TE materials, such as SnSe (PF $\approx 10\,\mu$W cm^{-1} K^{-2}) [36] and PbTe (PF $\approx 25\,\mu$W cm^{-1} K^{-2}) [3]. After applying a magnetic field, the PF gradually decreases with an increasing magnetic field in the temperature range from 49 K to 380 K, but remains almost unchanged below 49 K. The insets of Figs. 4(c) and 4(d) exhibit the magneto-PF [PF(0)/PF(B)–1] under a magnetic field of 9 T. Its maximum of 0.57 at 300 K and 0.69 at 150 K are observed with the magnetic field applied along the [100] and [100] crystal directions, respectively, which is possibly attributed to the fact that magnetic frustration is more easily suppressed with a magnetic field applied along the [100] crystal direction, in line with M-H [Fig. 1(d) and Supplemental Material Fig. S1 [35]).

Although the magnetism-enhanced S has been observed in many materials, it is still an intriguing academic viewpoint and has not been considered for practical application in enhancing TE performance. Two reasons may be responsible: one is that the increased resistivity compensates for the increased S, leading to a tiny improvement on TE performance. Surprisingly, originating from the large magnetic entropy induced by strong magnetic frustration, the magneto-S is significantly larger than the magneto-ρ, which leads to a

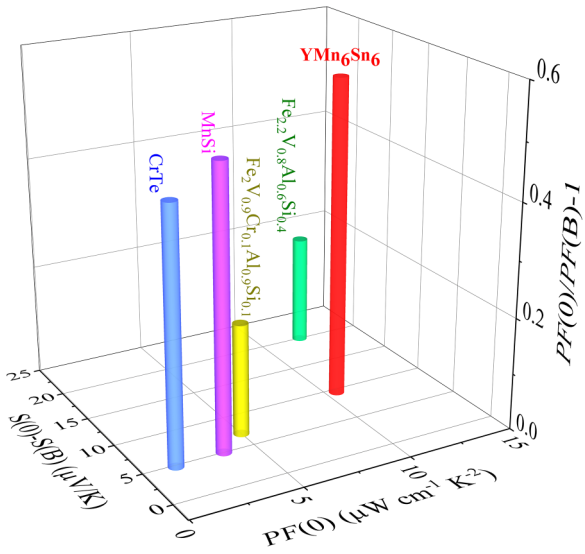

FIG. 5. Comparing peak PF(0), $S(0)$–$S(B)$, and [PF(0)/PF(B)–1] of YMn_6Sn_6 with other typical materials enhanced by magnetism.

large magnetism-enhanced PF in the kagome antiferromagnet YMn_6Sn_6. Figure 5 shows YMn_6Sn_6, PF(0), and $S(0)$–$S(B)$ for some typical materials with TE performance enhanced by magnetism [10,37,38], which all have been confirmed through applying the external magnetic field. It is worth noting that the magnetism-enhanced PF for the kagome antiferromagnet YMn_6Sn_6 far exceeds that of other typical materials. The second reason is that the magnetism-enhanced S often occurs over a narrow temperature range and quickly quenches below the magnetic transition temperature. For example, the magnetic fluctuation enhanced S extends only 5 K below the magnetic transition temperature for MnSi [37] and 85 K for $Fe_{2.2}V_{0.8}Al_{0.6}Si_{0.4}$ [10]. However, a significant magnetic entropy enhanced S can be observed in an extremely broad temperature range from around 50 K to above 380 K due to the strong interplanar magnetic frustration of the antiferromagnetic kagome lattice. Overall, these results suggest that the strong magnetic frustration of a kagome lattice can enhance the S and TE performance more significantly in a much broader temperature range, indicating a greater practical application value of related materials.

IV. CONCLUSION

In summary, the TE properties of the antiferromagnetically coupled kagome lattice YMn_6Sn_6 were studied. Compared with the previous reported materials, with a magnetism-enhanced S that was only observed near the magnetic transition temperature, the S of the kagome lattice YMn_6Sn_6 is significantly enhanced by the interplanar magnetic frustration in a much broader temperature range, which is more friendly for practical application. In addition, the phonon drag also contributes to the enhancement of the S, which is more significant near the phonon peak and is certified by the fitting of thermal conductivity and heat capacity. Owing to the enhancement of the S through magnetic frustration and phonon drag, the maximum PF of YMn_6Sn_6 reaches 10.5 $\mu W\,cm^{-1}\,K^{-2}$, which is comparable with those of state-of-the-art TE materials. Moreover, the PF is enhanced by 57% through the magnetic frustration in YMn_6Sn_6 at room temperature, which is much larger than the magnetism-enhanced PF of other materials reported so far. These results suggest that an antiferromagnetic kagome lattice is an ideal guidance system for exploring other excellent TE materials enhanced by magnetic frustration.

All data supporting the plots within this work and the findings of this study are available from the corresponding author upon request.

ACKNOWLEDGMENTS

This work was financially supported in part by the National Natural Science Foundation of China (Grants No. 52125103, No. 52071041, and No. 12204072), the National Key Research and Development Program of the Ministry of Science and Technology of China (Grant No. 2019YFA0704901), and the China Postdoctoral Science Foundation (Grant No. 2021M700611). The authors acknowledge the support of the Analytical and Testing Center of Chongqing University for providing assistance with sample characterization and measurement of transport properties.

[1] L. D. Hicks and M. S. Dresselhaus, Thermoelectric figure of merit of a one-dimensional conductor, Phys. Rev. B **47**, 16631 (1993).

[2] J. P. Heremans, V. Jovovic, E. S. Toberer, A. Saramat, K. Kurosaki, A. Charoenphakdee, S. Yamanaka, and G. J. Snyder, Enhancement of thermoelectric efficiency in PbTe by distortion of the electronic density of states, Science **321**, 554 (2008).

[3] Y. Z. Pei, X. Y. Shi, A. LaLonde, H. Wang, L. D. Chen, and G. J. Snyder, Convergence of electronic bands for high performance bulk thermoelectrics, Nature (London) **473**, 66 (2011).

[4] W. Liu, X. J. Tan, K. Yin, H. Liu, X. Tang, J. Shi, Q. Zhang, and C. Uher, Convergence of conduction bands as a means of enhancing thermoelectric performance of n-type solid solutions, Phys. Rev. Lett. **108**, 166601 (2012).

[5] K. Biswas, J. Q. He, I. D. Blum, C. I. Wu, T. P. Hogan, D. N. Seidman, V. P. Dravid, and M. G. Kanatzidis, High-performance bulk thermoelectrics with all-scale hierarchical architectures, Nature (London) **489**, 414 (2012).

[6] M. V. Costache, G. Bridoux, I. Neumann, and S. O. Valenzuela, Magnon-drag thermopile, Nat. Mater. **11**, 199 (2011).

[7] K. Vandaele, S. J. Watzman, B. Flebus, A. Prakash, Y. Zheng, S. R. Boona, and J. P. Heremans, Thermal spin transport and energy conversion, Mater. Today Phys. **1**, 39 (2017).

[8] S. R. Boona, S. J. Watzman, and J. P. Heremans, Research update: Utilizing magnetization dynamics in solid-state thermal energy conversion, APL Mater. **4**, 104502 (2016).

[9] Y. Zheng, T. Lu, Md. M. H. Polash, M. Rasoulianboroujeni, N. Liu, M. E. Manley, Y. Deng, P. J. Sun, X. L. Chen, R.

P. Hermann, D. Vashaee, J. P. Heremans, and H. Zhao, Paramagnon drag in high thermoelectric figure of merit Li-doped MnTe, Sci. Adv. **5**, eaat9461 (2019).

[10] N. Tsujii, A. Nishide, J. Hayakawa, and T. Mori, Observation of enhanced thermopower due to spin fluctuation in weak itinerant ferromagnet, Sci. Adv. **5**, eaat5935 (2019).

[11] W. Y. Zhao, Z. Y. Liu, Z. G. Sun, Q. J. Zhang, P. Wei, X. Mu, H. Y. Zhou, C. C. Li, S. F. Ma, D. Q. He, P. X. Ji, W. T. Zhu, X. L. Nie, X. L. Su, X. F. Tang, B. G. Shen, X. L. Dong, J. H. Yang, Y. Liu, and J. Shi, Superparamagnetic enhancement of thermoelectric performance, Nature (London) **549**, 247 (2017).

[12] I. Terasaki, Y. Sasago, and K. Uchinokura, Large thermoelectric power in $NaCo_2O_4$ single crystals, Phys. Rev. B **56**, R12685 (1997).

[13] Y. Y. Wang, N. S. Rogado, R. J. Cava, and N. P. Ong, Spin entropy as the likely source of enhanced thermopower in $Na_xCo_2O_4$, Nature (London) **423**, 425 (2003).

[14] M. R. Peterson and B. S. Shastry, Kelvin formula for thermopower, Phys. Rev. B **82**, 195105 (2010).

[15] P. J. Sun, K. R. Kumar, M. Lyu, Z. Wang, J. S. Xiang, and W. Q. Zhang, Generic Seebeck effect from spin entropy, Innovation **2**, 100101 (2021).

[16] N. J. Ghimire and I. I. Mazin, Topology and correlations on the kagome lattice, Nat. Mater. **19**, 137 (2020).

[17] J. X. Yin *et al.*, Quantum-limit Chern topological magnetism in $TbMn_6Sn_6$, Nature (London) **583**, 533 (2020).

[18] L. Ye, M. Kang, J. Liu, F. von Cube, C. R. Wicker, T. Suzuki, C. Jozwiak, A. Bostwick, E. Rotenberg, D. C. Bell, L. Fu, R. Comin, and J. G. Checkelsky, Massive Dirac fermions in a ferromagnetic kagome metal, Nature (London) **555**, 638 (2018).

[19] Z. Lin, J. Choi, Q. Zhang, W. Qin, S. Yi, P. Wang, L. Li, Y. Wang, H. Zhang, Z. Sun, L. Wei, S. Zhang, T. Guo, Q. Lu, J. Cho, C. Zeng, and Z. Y. Zhang, Flatbands and emergent ferromagnetic ordering in Fe_3Sn_2 kagome lattices, Phys. Rev. Lett. **121**, 096401 (2018).

[20] M. Kang *et al.*, Dirac fermions and flat bands in the ideal kagome metal FeSn, Nat. Mater. **19**, 163 (2020).

[21] E. Liu *et al.*, Giant anomalous Hall effect in a ferromagnetic kagome-lattice semimetal, Nat. Phys. **14**, 1125 (2018).

[22] D. F. Liu, A. J. Liang, E. K. Liu, Q. N. Xu, Y. W. Li, C. Chen, D. Pei, W. J. Shi, S. K. Mo, P. Dudin, T. Kim, C. Cacho, G. Li, Y. Sun, L. X. Yang, Z. K. Liu, S. S. P. Parkin, C. Felser, and Y. L. Chen, Magnetic Weyl semimetal phase in a kagomé crystal, Science **365**, 1282 (2019).

[23] K. Kuroda *et al.*, Evidence for magnetic Weyl fermions in a correlated metal, Nat. Mater. **16**, 1090 (2017).

[24] F. H. Yu, T. Wu, Z. Y. Wang, B. Lei, W. Z. Zhuo, J. J. Ying, and X. H. Chen, Concurrence of anomalous Hall effect and charge density wave in a superconducting topological kagome metal, Phys. Rev. B **104**, L041103 (2021).

[25] S. Roychowdhury, A. M. Ochs, S. N. Guin, K. Samanta, J. Noky, C. Shekhar, M. G. Vergniory, J. E. Goldberger, and C. Felser, Large room temperature anomalous transverse thermoelectric effect in kagome antiferromagnet YMn_6Sn_6, Adv. Mater. **34**, 2201350 (2022).

[26] N. J. Ghimire, R. L. Dally, L. Poudel, D. C. Jones, D. Michel, N. T. Magar, M. Bleuel, M. A. Mcguire, J. S. Jiang, J. F. Mitchell, J. W. Lynn, and I. I. Mazin, Competing magnetic phases and fluctuation-driven scalar spin chirality in the kagome metal YMn_6Sn_6, Sci. Adv. **6**, eabe2680 (2020).

[27] P. E. Siegfried, H. Bhandari, D. C. Jones, M. P. Ghimire, R. L. Dally, L. Poudel, M. Bleuel, J. W. Lynn, I. I. Mazin, and N. J. Ghimire, Magnetization-driven Lifshitz transition and charge-spin coupling in the kagome metal YMn_6Sn_6, Commun. Phys. **5**, 58 (2022).

[28] Q. Wang, Q. Yin, S. Fujitsu, H. Hosono, and H. Lei, Near-room-temperature giant topological Hall effect in antiferromagnetic kagome metal YMn_6Sn_6, Phys. Rev. B **103**, 014416 (2021).

[29] S. Lee, A. Pirogov, M. Kang, K. Jang, M. Yonemura, T. Kamiyama, S. W. Cheong, F. Gozzo, N. Shin, H. Kimura, Y. Noda, and J. G. Park, Giant magneto-elastic coupling in multiferroic hexagonal manganites, Nature (London) **451**, 805 (2008).

[30] M. Long, A. R. Wazzan, and R. Stern, Magneto-elastic interactions in gadolinium, Phys. Rev. **178**, 775 (1969).

[31] R. L. Dally, J. W. Lynn, N. J. Ghimire, D. Michel, P. Siegfried, and I. I. Mazin, Chiral properties of the zero-field spiral state and field-induced magnetic phases of the itinerant kagome metal YMn_6Sn_6, Phys. Rev. B **103**, 094413 (2021).

[32] M. Wagner-Reetz, D. Kasinathan, W. Schnelle, R. Cardoso-Gil, H. Rosner, Y. Grin, and P. Gille, Phonon-drag effect in $FeGa_3$, Phys. Rev. B **90**, 195206 (2014).

[33] T. M. Tritt, *Thermal Conductivity: Theory, Properties, and Applications* (Kluwer Academic/Plenum Publishers, New York, 2005).

[34] Y. Liu, Z. Hu, M. Abeykoon, E. Stavitski, K. Attenkofer, E. D. Bauer, and C. Petrovic, Polaronic transport and thermoelectricity in $Mn_3Si_2Te_6$ single crystals, Phys. Rev. B **103**, 245122 (2021).

[35] See Supplemental Material at http://link.aps.org/supplemental/10.1103/PhysRevB.108.155135 for Isothermal magnetizations and the temperature-dependent magneto-resistivity.

[36] L. D. Zhao, S. Lo, Y. Zhang, H. Sun, G. Tan, C. Uher, C. Wolverton, V. P. Dravid, and M. G. Kanatzidis, Ultralow thermal conductivity and high thermoelectric figure of merit in SnSe crystals, Nature (London) **508**, 373 (2014).

[37] Y. Hirokane, Y. Tomioka, Y. Imai, A. Maeda, and Y. Onose, Longitudinal and transverse thermoelectric transport in MnSi, Phys. Rev. B **93**, 014436 (2016).

[38] M. M. H. Polash and D. Vashaee, Spin fluctuations yield zT enhancement in ferromagnets, iScience **24**, 103356 (2021).